RSC Advances

PAPER

View Article Online
View Journal | View Issue

Cite this: *RSC Adv.*, 2023, **13**, 2467

Controllable formation of amorphous structure to improve the oxygen evolution reaction performance of a CoNi LDH†

You Ye,[a] Yan Shan,*[a] Hongli Zhu,[b] Kezheng Chen[a] and Xuegang Yu *[a]

Received 13th October 2022
Accepted 6th January 2023

DOI: 10.1039/d2ra06447b

rsc.li/rsc-advances

The morphology design of layered double hydroxides (LDHs) is an important way to determine the catalytic performance of LDH materials. A novel structure of CoNi LDH sheets with amorphous structure on the edge was prepared by electrooxidation. It was characterized by XRD, SEM, TEM and XPS. It was found that during the electrooxidation, some of the Co^{2+} ions were oxidized to Co^{3+} to form amorphous CoOOH intermediates, which promoted the OER performance. The electrochemical test results show that CoNi LDH treated by electrooxidation for 6 hours has an ultra-low overpotential of 206 mV at a current density of 10 mA cm^{-2}, and can work stably under alkaline conditions for more than 10 hours. This work suggests that introducing an amorphous structure on LDH through electrooxidation produces abundant active sites, which is an easy and efficient method to improve the OER performance of CoNi LDHs.

1. Introduction

With the increasing consumption of fossil fuels, fossil energy is on the verge of exhaustion, and people are facing a serious energy crisis. So the scientists have to develop renewable and pollution-free energy to replace traditional energy.[1–5] Hydrogen energy is one of the most promising potential alternatives to traditional fossil fuels due to its high specific energy density, environmental benignity and abundant sources.[6–9] The electrolysis of water is an effective way for large-scale hydrogen production.[10,11] Hydrogen evolution reaction (HER) and oxygen evolution reaction[12–15] are the two parts of water splitting, and both of them need suitable catalysts to achieve excellent catalytic performance and good stability. Compared with HER, the OER possesses low energy conversion efficiency and sluggish kinetics, due to a four-electron process at the anode.[16,17] The development of high-efficiency OER electrocatalysts can greatly improve the hydrogen production rate and energy conversion efficiency of water splitting. To date, noble-metal-based materials[12,18,19] are considered as the most efficient catalysts toward water splitting (*i.e.* Pt/C for HER and RuO_2 for OER). Nevertheless, the high cost and scarcity limit their widespread applications. As consequence, it is necessary to design and fabricate high-efficiency non-precious-metal-based catalysts to overcome this defect.

To date, earth-abundant 3d transition[20,21] metals have been extensively researched for water electrolysis. Among of the superior electrocatalysts, CoNi layered double hydroxide (LDH),[22–24] which have been notably validated as attainable electrocatalyst for OER due to their flexible adjustability in chemical composition, morphology and thickness, has aroused widespread concern among researchers. Chu *et al.* reported a hybrid Ni_3S_2/vertical graphene@CoNi LDH catalyst. The introduction of vertical graphene could promote charge and ion transport, and could form optimized two-dimensional heterostructure.[24] Tian *et al.* prepared CoNi-LDH with nanobundle-like structure as an efficient catalyst for OER.[25] This catalyst is a novel class of mesoporous structure with high specific surface area, and it show an overpotential value of 266 mV to reach 10 mA cm^{-2} current density. Feng *et al.* studied CoNi-LDH with nanoflower structure rich in oxygen vacancies.[26] This LDH material can be slightly etched to obtain an open 3D structure through a simple solvothermal method and can provide a large specific surface area and abundant oxygen vacancies, and it show overpotential of 260 mV at 10 mA cm^{-2}. Tian *et al.* reported a core branch Co_3O_4@CoNi-LDH of OER catalyst. Co_3O_4 is introduced through metal organic frameworks template, and CoNi-LDH is indirectly loaded through atomic layer deposition technology. There are coupling interactions between these two components, and the 3D structure constructed together significantly improves the catalytic performance of OER.[27] Xu *et al.* presented *in situ* growth of brush like Co_3S_4@CoNi-LDH electrocatalyst. The prepared catalyst is convenient for charge transfer due to its unique structure and has a large specific surface area. The *in situ* growth method ensures the stability of

[a]*Lab of Functional and Biomedical Nanomaterials, College of Materials Science and Engineering, Qingdao University of Science and Technology, Qingdao 266042, China. E-mail: yuxuegang@qust.edu.cn; shanyan@qust.edu.cn; Fax: +86-532-84023616; Tel: +86-532-84023616*

[b]*Institute 53 of China's Ordnance Industry, Jinan 250031, China*

† Electronic supplementary information (ESI) available. See DOI: https://doi.org/10.1039/d2ra06447b

the catalyst. The synergistic effect between Co_3S_4 and NiCo-LDH is also one of the reasons for the high-efficiency OER catalytic activity.[28] Hu *et al.* found the hybrid $Ti_3C_2T_x$ MXene@CoNi LDH has excellent OER performance. $Ti_3C_2T_x$ MXene as support has prominent electronic coupling and strong interfacial interaction, and the OER activity of CoNi LDH can be further enhanced.[29] To sum up, CoNi-LDH can improve the catalytic efficiency in the OER process However, the catalytic activity of CoNi-LDH itself is insufficient, and few people have further studied it. Herein, this research adopts a simple and gentle method to fully expose the catalytic active sites to solve the above problems.

In this work, we have developed a CoNi double hydroxide on nickel foam by hydrothermal method. Then CoNi double hydroxide was modified by electrooxidation, which can obtain an amorphous heterogenous structure with plentiful active sites. The emerge of amorphous structure can adjust the interface structure and significantly improve the density of catalytic active sites, which provides an opportunity to improve the catalytic performance. Finally, the coexistence of amorphous structure and crystal structure show better OER performance than single crystal structure, which provides a new way to improve LDH catalyst performance and a good prospect in industrial energy storage.

2. Experimental section

2.1 Materials

Cobalt nitrate hexahydrate ($Co(NO_3)_2$), ethanol (CH_3CH_2OH), urea ($CO(NH_2)_2$), ammonium fluoride (NH_4F) and potassium hydroxide (KOH) were purchased from Sinopharm Chemical Reagent Co. Ltd. All above chemicals were of analytic grade and used directly without further purification. Ni foam (NF) was bought from Qingdao Zhengye Chemical Reagent Co. Ltd.

2.2 Synthesis of CoNi-LDH-Ex@NF

Ni foam was sonicated in hydrochloric acid, ethanol and DI for 15 min respectively, to eliminate the interference of surface impurities, and then the Ni foam was dried under vacuum at 60 °C. 0.5 mmol $Co(NO_3)_2$ was dissolved in 50 mL DI water. Then 2 mmol NH_4F and 5 mmol urea were added. The solution was vigorous stirred for 15 min and ultrasonic treatment for 15 min, it was transferred into a 100 mL Teflon-lined autoclave, where the cleaned Ni foam (1*5 cm^2) was placed at a 45° angle to the bottom. Then the sealed autoclave was kept temperature at 120 °C for 6 h to synthesize CoNi-LDH@NF. The obtained CoNi-LDH@NF was rinsed with DI water and ethanol for more than three times, and kept in vacuum at 60 °C for 6 h to dry. After drying, CoNi-LDH@NF was electrooxidized at the potential of 1.7 V (*vs.* RHE) in 1 M KOH solution to obtain CoNi-LDH-Ex@NF (x is the processing time of electrooxidation, and the sample CoNi-LDH-E0@NF represents CoNi-LDH@NF without electrooxidation). The electrooxidation process was conducted on a CHI660E electrochemical workstation (CH Instruments, Inc, shanghai),using a standard three-electrode system. The CoNi-LDH@NF was working electrolyte, platinum wire (CHI115) was used as counter electrode, and Hg/HgO electrode was served as reference electrode. The synthesis process of CoNi-LDH-Ex@NF is shown in Fig. 1. At first, CoNi-LDH was loaded on a piece of clean foam NF by hydrothermal reaction. Secondly, the prepared CoNi-LDH@NF was electrooxidized to obtain the desired morphology.

2.3 Material characterizations

X-ray diffraction (XRD, D/MAX/2500PC, Japan) was used to characterize the phase analysis of samples. The surface morphologies, structure and element composition of samples were observed by scanning electron microscopy (SEM, JSM-6700F, Japan) with energy-dispersive X-ray spectroscope and transmission electron microscopy (TEM, JEM-2100PLUS, Japan). The composition and chemical valence states of the elements were detected by X-ray photoelectron spectroscopy (XPS, ESCALAB XI+, Thermo fisher).

2.4 Electrochemical measurements

Electrochemical workstation (CH Instruments, Inc, shanghai) is used for electrochemical measurements. The experiment was carried out with a three electrode system in 1 M KOH electrolyte. All prepared CoNi-LDH-Ex@NF (1 cm*0.5 cm) were used as the

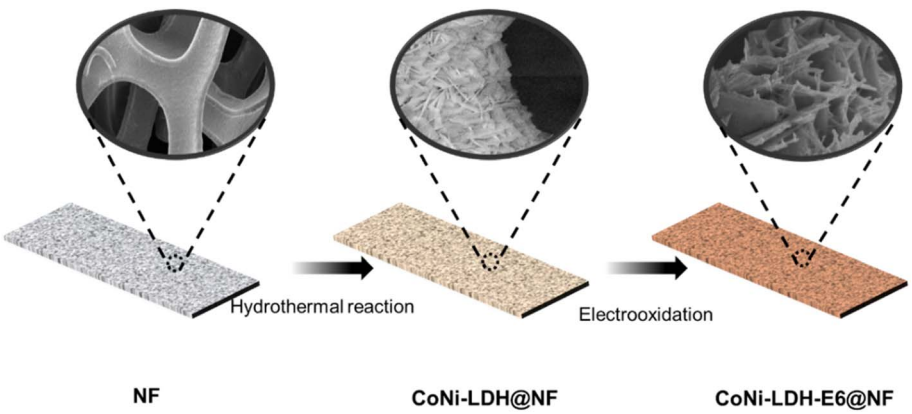

Fig. 1 Schematic illustration of the preparation for CoNi-LDH-E6@NF composites.

working electrode with Ag/AgCl reference electrode (CHI111, 0.222 V *vs.* RHE, at 25 °C) as the reference electrode and platinum wire (CHI115) as the counter electrode. Linear sweep voltammetry (LSV) was tested from 0.6 V to 0 V (*vs.* Ag/AgCl) with a scan rate of 5 mV s^{-1} for avoiding the interference of oxidation peak of Ni foam. Electrochemical impedance spectroscopy (EIS) measurements were carried out in the frequency from 100 000 to 0.01 Hz with an AC potential amplitude of 5 mV, and the applied voltage was 0.5 V (*vs.* Ag/AgCl). Electrochemical active surface area (ECSA) is estimated by electric double layer capacitor (Cdl) and the electrical double layer capacitor was measured from double-layer charging curves using cyclic voltammetry (CV) at scan rates from 20 to 100 mV s^{-1} in a non-faradaic potential range of 0.05–0.15 V (*vs.* Ag/AgCl). To test stability of material, chronoamperometric measurements were got at a constant current density of 9 mA cm^{-2} for 10 h. Tafel slope is calculated by the following formula: $\eta = b^{*}\log j + a$, where η represents the overpotential, b refers to the Tafel slope, and j is the current density. The potential of Ag/AgCl converted to RHE follows Nernst equation: $E_{RHE} = E_{Ag/AgCl} + 0.059\ pH + 0.222$. The overpotential ($\eta$) is calculated by the following simple formula: $\eta = E_{RHE} - 1.23(V)$.

3. Results and discussion

Through the simple hydrothermal method and electrooxidation method, CoNi-LDH-Ex@NF was successfully synthesized. The structural information of CoNi-LDH-Ex@NF was characterized by XRD. Fig. 2a shows the XRD patterns of the CoNi-LDH@NF with different electrooxidation time treatment. All samples show three sturdy and sharp peaks at 44.6°, 51.9°, and 76.4°, corresponding to (110), (200), and (220) of Ni (JCPDS No.01-1258). Moreover, all samples have poor crystallization, due to the fact one broad diffraction peak is located in each sample. And the proportion of broad peak was increased to some extent with the electrooxidation time. This result indicates that there is a small amount of amorphous structure in the samples after hydrothermal reaction, and the degree of amorphization of the samples increases greatly after the electro oxidation process. There is low level of crystalline phase of CoNi-LDH in the CoNi-LDH-Ex@NF, and it is the reason why the diffraction peak of CoNi-LDH crystal phase is not observed in XRD patterns. In order to determine the main components of the sample on NF, the powder in the autoclave were collected for XRD characterization. The XRD pattern of the CoNi-LDH powder without electrooxidation was shown in Fig. 2b, and the pattern is matched the standard pattern (JCPDS No.30-0443, JCPDS No.43-1003, JCPDS No.14-0117) and the results reveal that $Co(OH)_2$, Co_3O_4, CoOOH and $Ni(OH)_2$ were included in the powder. In the hydrothermal reaction, $Co(OH)_2$ may be directly formed by precipitation reaction (eqn (1)), while Co_3O_4 may be a compound of high valent cobalt formed by oxidation of a small part of Co^{2+} (eqn (2)), and $Ni(OH)_2$ may be formed by oxidation–reduction reaction between elemental Ni and high valent Co and precipitation reaction with OH^-(eqn (3)). Therefore, the components of the prepared compound are Ni^{2+} and Co elements in different oxidation states as the cation layer, and OH^- and oxygen ions as the adjacent anion layer. The cation layer and the anion layer are naturally stacked adjacent to each other to form CoNi-LDH. These results successfully prove that CoNi-LDH is loaded on NF, which makes CoNi-LDH have a suitable place for electrooxidation.

$$Co^{2+} + OH^- \rightarrow Co(OH)_2 \quad (1)$$

$$3Co^{2+} + 2O_2 \rightarrow Co_3O_4 \quad (2)$$

$$2Co^{3+} + Ni + 6OH^- \rightarrow Ni(OH)_2 + 2Co(OH)_2 \quad (3)$$

Fig. 3a and b are SEM images of NF, and it can be seen that the NF skeleton has a certain 3D structure and the surface is relatively smooth and clean. Fig. 3c and d display SEM images of the surface morphology of CoNi-LDH-E0@NF. Under the hydrothermal reaction at 120 °C for 6 h, sheet structure CoNi LDH was successfully and uniformly loaded on NF. It can be seen that the thickness of the CoNi LDH sheet is about 450 nm, and the surface of sheets is relatively flat. The reason for this may be that the LDH materials prepared by hydrothermal method inevitably make the nanosheets stack to form large sheet. Fig. 3e and f show the SEM images of the sample of CoNi-LDH-E6@NF. Notice that, compared with CoNi-LDH-E0@NF,

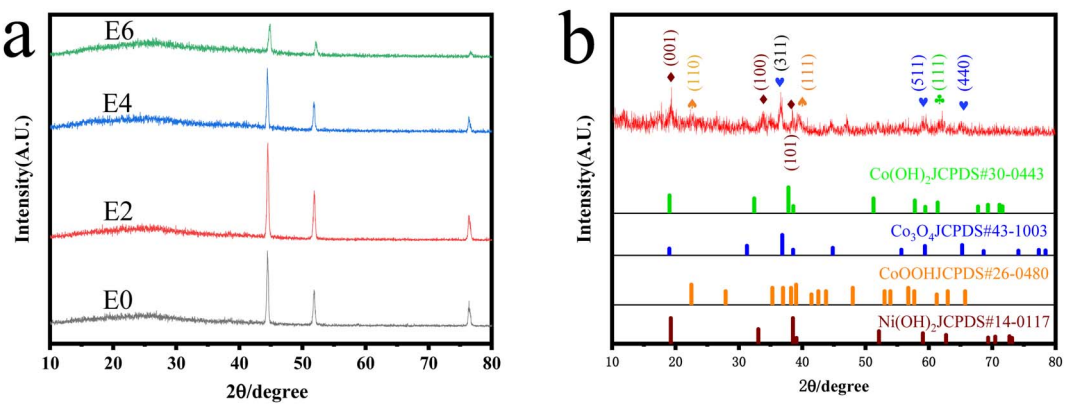

Fig. 2 (a) XRD patterns of the CoNi-LDH@NF with different electrooxidation time treatment, (b) XRD pattern of the CoNi-LDH powder.

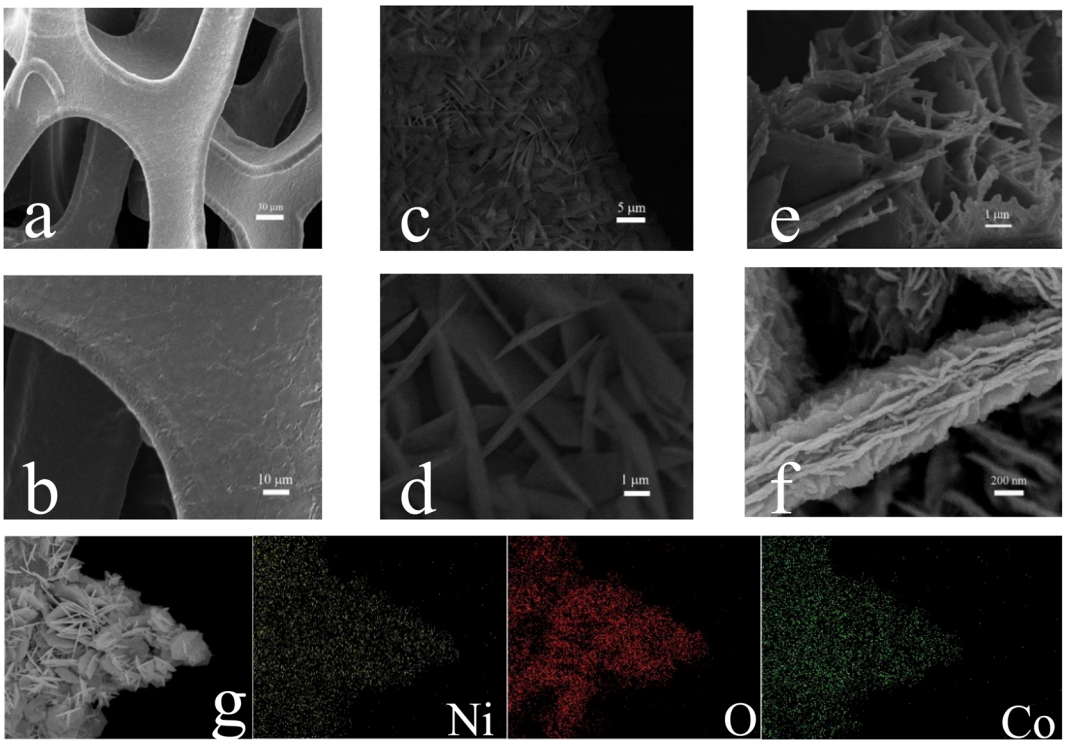

Fig. 3 (a and b) SEM images of NF with different magnifications, (c and d) SEM images of CoNi-LDH-E0@NF with different magnifications, (e and f) SEM images of CoNi-LDH-E6@NF with different magnifications, (g) elemental mapping of CoNi-LDH-E6@NF.

the edges of each CoNi-LDH-E6@NF nanosheets are very rough, where nanorods emerge.

In addition, the overall structure of CoNi-LDH-E6@NF has not been damaged, and the size has hardly changed, maintaining the original 2D structure. The presence of a large number of uniform nanosheets and nanorods will expand the specific surface area of the material and present 3D nanostructures, which will expose extra active sites. Moreover, obviously, it can be further seen that CoNi-LDH materials prepared by hydrothermal method have a stacking effect, and large nanosheets are formed by stacking small nanosheets with a thickness of 40 nm. The thickness of CoNi-LDH-E6@NF sheets is about 650 nm, 200 nm more than that of CoNi-LDH-E0@NF sheets. This shows that the electrooxidation treatment opens the gap between the nanosheets and solves the stacking effect of LDH materials. The SEM images can clearly show that the CoNi-LDH material will undergo certain morphological adjustment along its growth direction, that is, the edge, after electrooxidation.[30] In addition, the elements Co, Ni and O are uniformly distributed on the whole CoNi-LDH-E6@NF electrode, as indicated by Fig. 3g.

To confirm the difference of surface structure before and after electrooxidation, the internal structure and morphology of CoNi-LDH-E0@NF (Fig. S1†) and CoNi-LDH-E6@NF (Fig. 4) are characterized by transmission electron microscopy. As shown in the Fig. S1,† the CoNi-LDH nanosheet (CoNi-LDH-E0@NF) without electrooxidation treatment is relatively smooth, especially in the edge area. After electrooxidation treatment, from the Fig. 4a, it can be seen that the edge of CoNi-LDH nanosheet (CoNi-LDH-E6@NF) is rough, and a layer of amorphous structure may be wrapped around the edge of the nanosheet. As shown in Fig. 4b, some CoNi-LDH-E6@NF nanosheets have holes, which makes the nanosheets have a network structure and a larger specific surface area. Therefore, it was found that the morphology of the nanosheets was damaged to a certain extent after electrooxidation treatment. This newly formed amorphous structure and porous structure expose more active sites and is conducive to better contact between active sites and electrolytes in the OER process. The HRTEM images of CoNi-LDH-E6@NF were shown in Fig. 4c and d. As can be seen, the nanosheets consists of well-defined crystalline phase in the core part, and an ultrathin layer (~5 nm) of amorphous nanodomains on the surface. In addition, the lattice fringe of the CoNi-LDH-E6@NF nanosheets was 0.2659 nm, corresponding to the (101) plane (JCPDS No.38-0715).[22,31,32] This result further indicates that LDH is successfully and uniformly loaded on NF.

In order to further determine the chemical states and valence states of CoNi-LDH-E6@NF and understand the transformation of components before and after electrooxidation, the sample was characterized by X-ray photoelectron spectroscopy (XPS). As shown in the Fig. 5a, the XPS survey spectrum of CoNi-LDH-E6@NF reveals the presence of Ni, Co, O and C species. In the Co 2p region (Fig. 5b), the peaks at the binding energies (BEs) of 781.1 and 785.7 eV were assigned to $2p_{3/2}$ of Co^{3+} and Co^{2+} respectively; While the peak at 796.4 and 798.6 eV belong to $2p_{1/2}$ of Co^{3+} and Co^{2+} respectively; The other peaks at 804.6 and 790.6 eV corresponded to satellite peaks. Compared with the XPS survey spectrum of CoNi-LDH-E0@NF (Fig. 6b), the peaks of Co^{2+} were decreased, which indicates the oxidation of

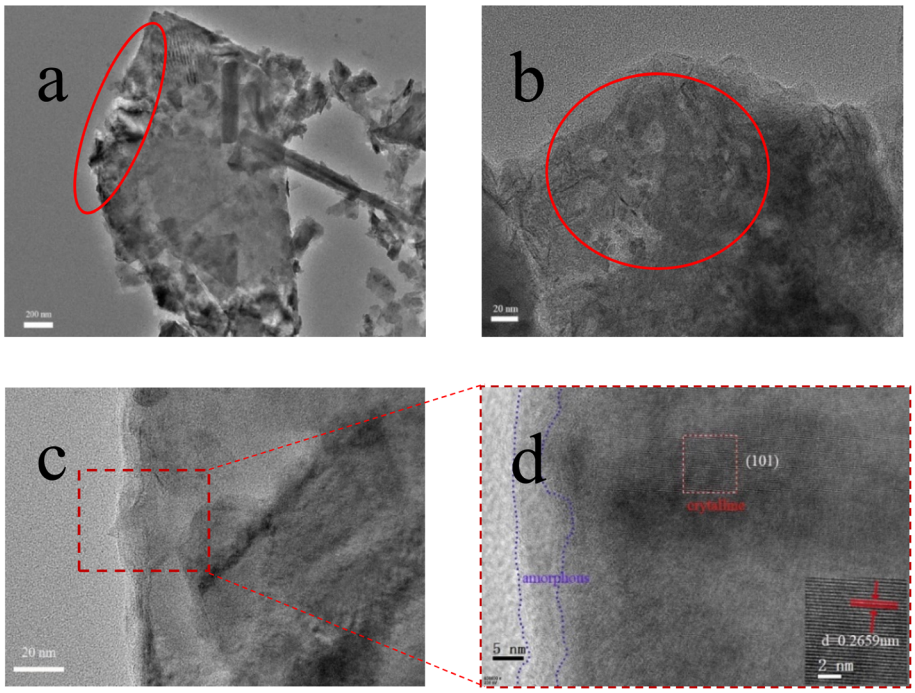

Fig. 4 (a and b) TEM images of CoNi-LDH-E6@NF with different magnifications, (c and d) HRTEM images of CoNi-LDH-E6@NF.

the element Co in the course of electrooxidation, and it explains the increase of amorphous materials. In Fig. 5c, the satellite peaks can be found with their binding energy at 862.0 and 880.0 eV, and the peaks at 855.9 and 873.5 eV belong to Ni $2p_{3/2}$ and $2p_{1/2}$ respectively, which shows the existence of Ni^{2+}. As shown in Fig. 5d, the peaks with binding energies of 529.3 eV,

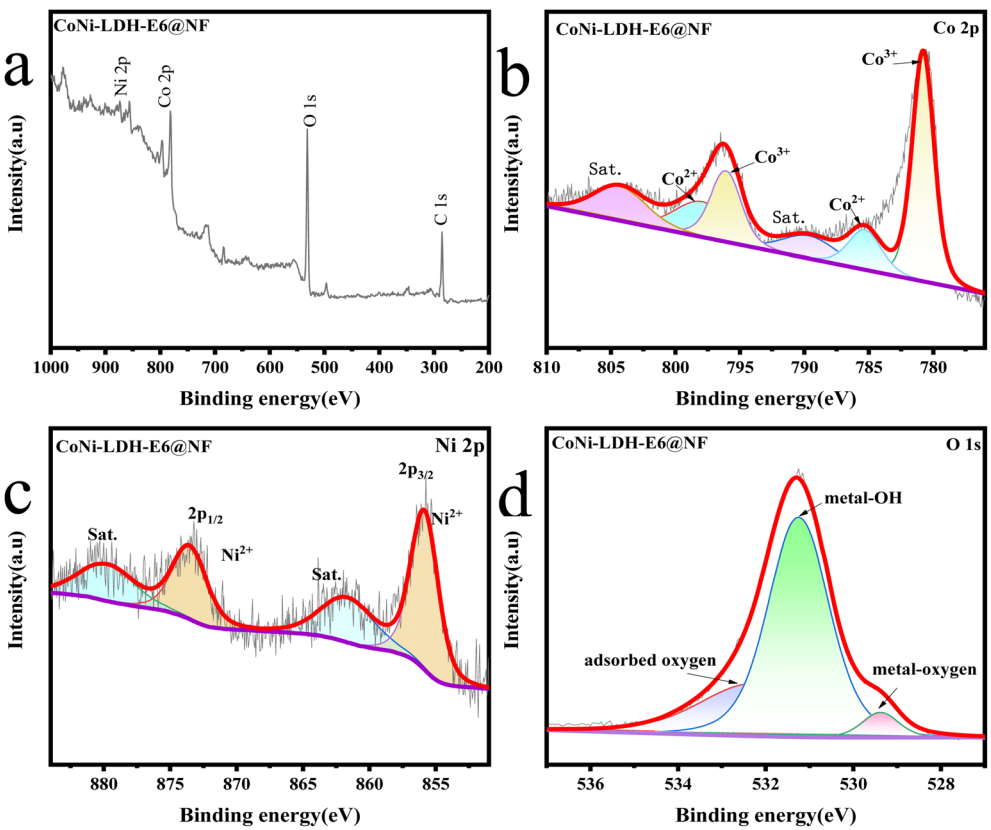

Fig. 5 (a) XPS spectra of CoNi-LDH-E6@NF, high-resolution XPS spectrum of (b) Co 2p, (c) Ni 2p, (d) O 1s.

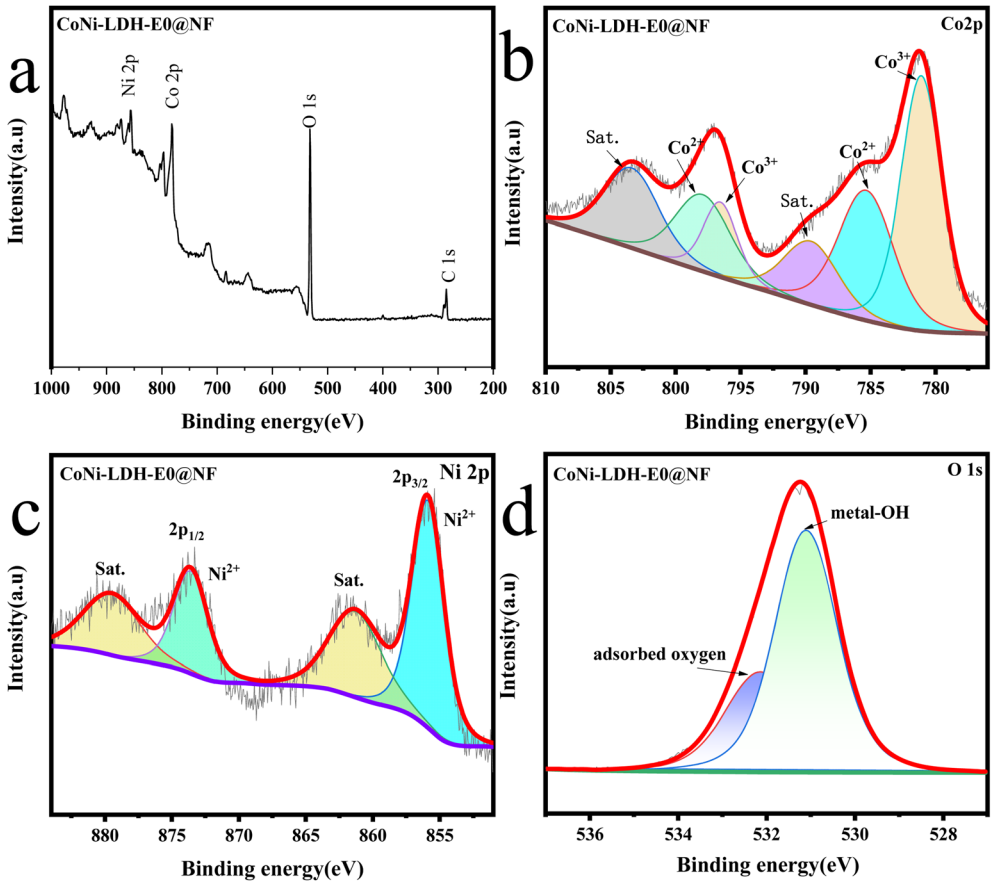

Fig. 6 (a) XPS spectra of CoNi-LDH-E0@NF, high-resolution XPS spectrum of (b) Co 2p, (c) Ni 2p, (d) O 1s.

531.2 eV and 532.2 eV are corresponded to the metal–oxygen, metal–OH and adsorbed oxygen, respectively.

Fig. 6 shows the XPS spectra of sample without electrooxidation treatment. As shown in Fig. 6a, the CoNi-LDH-E0@NF without electrooxidation also reveals the presence of Ni, Co, O and C species. It can be seen from Fig. 6c that the chemical state of element Ni is almost the same as that before electrooxidation treatment. For O 1s in Fig. 6d, the peak of metal–oxygen at 529.3 eV can't be observed, which may due to the low content of metal oxides, and it indicates that the electrooxidation process introduces some Co oxides into the amorphous structure. These results indicate that the valence of Co in the sample changes after electrooxidation during the surface experiment, and since Co is changing from bivalent to trivalent, the catalyst composition also has a change process. However, when the catalyst recombines to form new cobalt valence compounds, the growth rate of crystal nuclei is relatively slow. In the edge region of the nanosheet, the particles show that they do not repeat periodically in the three-dimensional space, and have the isotropic properties, which may be the reason for the formation of amorphous structure.

The electrochemical tests result of CoNi-LDH-Ex@NF and commercial RuO_2 are shown in the Fig. 7. From the LSV curve (Fig. 7a), it can be concluded that the OER performance of CoNi-LDH@NF is positively correlated with the electrooxidation treatment time. As in shown Fig. 7b, the Tafel plot of CoNi-LDH-E6@NF is 60.27 mV dec^{-1} in the overpotential region of 160–190 mV, which is smaller than those of CoNi-LDH-E0@NF, CoNi-LDH-E2@NF, CoNi-LDH-E4@NF, indicating that the CoNi-LDH-E6@NF sample has the superior catalytic kinetics for the OER process. Overpotential at 10 mA cm^{-2} was measured for the catalytic performance of the materials. As shown in Fig. 7c, with the increase of electrooxidation time, the OER performance of CoNi-LDH@NF is significantly improved. When the electrooxidation time of CoNi-LDH@NF is 6 h, the overpotential of CoNi-LDH@NF catalyst is the smallest (the overpotential is 206 mV), at the current density of 10 mA cm^{-2}. The electrochemical OER properties of CoNi-LDH-E6@NF and the corresponding results in some recent articles are compared in Table 1. The cyclic voltammetry curves of the samples are measured in the no faradaic processes interval, and the curves are used to fit the double-layer capacitance (C_{dl}) of the samples (Fig. S2†). In this way, the electrochemical active surface area (ECSA) of the samples can be calculated. As shown in Fig. 7d, the relationships between the scanning rate and the CV curve were drawn. It can be seen that the ECSA of each sample has little difference and it may be that the activity of these samples is related to their intrinsic activity. Stability is an important parameter to judge the properties of materials, which is the key factor in practical application. As presented in Fig. 7e, there are no obvious current decay is observed after 10 h occurred for CoNi-LDH-E6@NF. The electrochemical impedance spectroscopy (EIS) curves of the samples

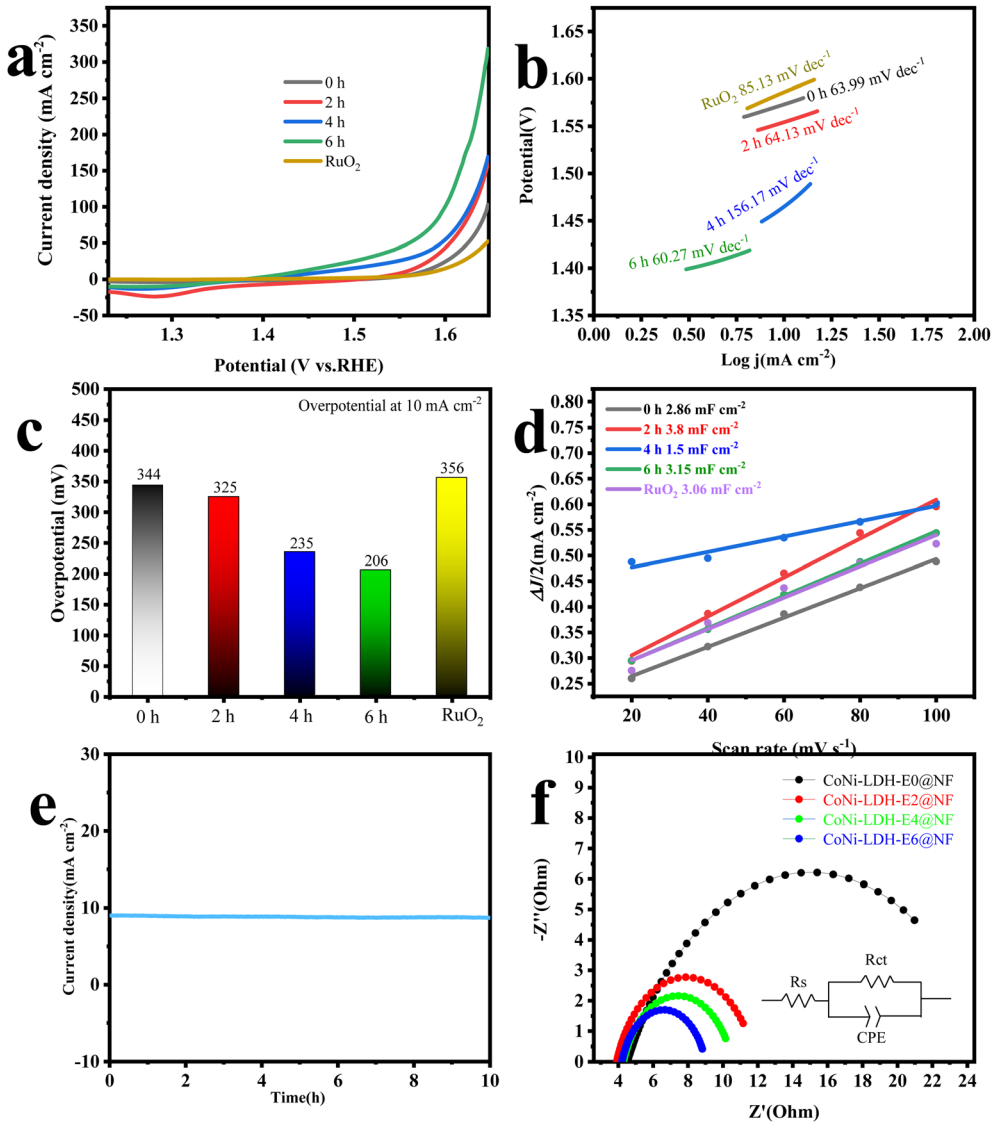

Fig. 7 (a) LSV curves of different samples and RuO_2; (b) Tafel plots derived from LSV curves; (c) overpotential of different samples and RuO_2 at the current density of 10 mA cm^{-2}; (d) capacitive currents at 0.1 V (*vs.* Ag/AgCl) as a function of scan rates; (e) i–t curve of CoNi-LDH-E6@NF; (f) EIS curves.

Table 1 Comparison of OER performance of CoNi-LDH-E6 catalyst with recently reported other electrocatalysts

Material	Electrolyte	η_{10}	Tafel slope	Ref.
NiFe LDHs	1 M KOH	307 mV	40 mV dec^{-1}	42
NiMn-LDH/C_3N_4	1 M KOH	316 mV	65 mV dec^{-1}	43
NiMn (Cl)-LDH	1 M KOH	420 mV	79 mV dec^{-1}	44
CoMn-LDH	1 M KOH	350 mV	43 mV dec^{-1}	45
CoCr LDHs	1 M KOH	417 mV	74 mV dec^{-1}	46
CoAl LDHs	1 M KOH	400 mV	83 mV dec^{-1}	47
CeO_2/NiFe LDH	1 M KOH	246 mV	65 mV dec^{-1}	48
Co–C@NiFe LDH	1 M KOH	249 mV	57.9 mV dec^{-1}	49
CoNi-LDH-E6@NF	1 M KOH	206 mV	60.27 mV dec^{-1}	This work

were measured to further study the effect of electrooxidation on the properties of the samples. The EIS spectra of CoNi LDH treated with four kinds of electrooxidation time are shown in the Fig. 7f. The sample with the lowest charge transfer resistors is CoNi-LDH-E6@NF, which indicates that the formation of amorphous structure can effectively enhance the charge transfer of materials.

The excellent electrochemical performance of CoNi-LDH-E6@NF may be attributed to the following reasons: firstly, LDH materials contain a large number of multivalent metal cations. These multivalent metal cations have redox features at a certain potential, which makes LDH materials with 2D layered structure have good charge transfer. During the electrochemical reactions process, the dynamic change of positive charges between layers will be balanced by the migration of intercalated anions in the interlayer space.[33–35] Secondly, NiOOH and CoOOH are suitable substances for OER,[36,37] while Ni and Co in LDH can be oxidized *in situ* to NiOOH and CoOOH under alkaline conditions, which is also the reason why CoNi-LDH is considered to be a catalyst for OER under alkaline conditions.

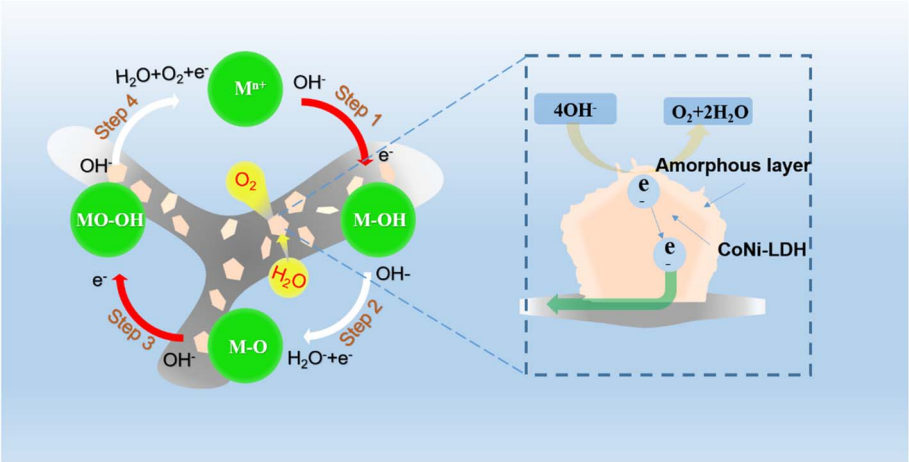

Fig. 8 The schematic illustration for OER.

In the OER process, the four-electron transfer process of transition metal-based catalyst under alkaline conditions is shown in Fig. 8. The M^{n+} goes through four processes, forming M–OH, M–O and MO–OH respectively by adsorbing OH^-, and finally producing O_2 (eqn (4)–(7)).[38]

$$M^{n+} + OH^- \rightarrow MOH + e^- \quad (4)$$

$$MOH + OH^- \rightarrow MO + H_2O + e^- \quad (5)$$

$$MO + OH^- \rightarrow MOOH + e^- \quad (6)$$

$$MOOH + OH^- \rightarrow M + O_2 + H_2O + e^- \quad (7)$$

Additionally, under alkaline conditions, the OER process is usually accompanied by proton-coupled electron transfer (eqn (8)).[37,39] The rich Co^{3+} in CoNi-LDH-E6@NF may lead to more extra charges to conduct proton and electron migration, and it makes the reaction more kinetic and lower energy barrier. In addition, the chemical properties of catalysts are mainly dominated by surface effects. The growth direction of LDH nanosheets is also due to the different coordination of atoms on the surface and edge. The lack of coordination edge has a great impact on the formation of nanosheets, which is also the active site of OER reaction. The Co^{2+} in the material is changed into Co^{3+} by electrooxidation, which makes the LDH edge atoms have larger coordination number and stronger surface effect. This makes CoNi-LDH-E6@NF more capable of adsorbing OH^-.

$$[Co^{III}–OH] \rightarrow [Co^{IV}–O] + H^+ + e^- \quad (8)$$

Thirdly, for general LDH materials, the active center may be covered up, which cannot play a catalytic role, and the OER performance of the materials will be reduced.[16,40] The amorphous structure of CoNi-LDH-E6@NF increases the specific surface area and forms a large reaction interface, which is conducive to the diffusion of electrolyte and the release of evolved gas bubbles.[41] Moreover, CoNi-LDH-E6 is directly grown on NF to obtain an integral electrode, which can avoid the use of binder such as Nafion, reduce resistance, promote electron transmission between electrode and electrolytic interface and improve catalytic activity. The above advantages may be the reasons for the excellent OER performance of LDH.

4. Conclusions

In this work, the coexistence of amorphous and crystalline structures by electrooxidation is proposed to improve the OER performance of CoNi LDH. The as-prepared CoNi-LDH-E6@NF displays excellent OER activity with ultralow overpotentials of 206 mV at $j = 10$ mA cm^{-2} and a small Tafel slope of 60.27 mV dec^{-1} in alkaline electrolyte, and the sample also exhibits good stability with working at 9 mA cm^{-2} current density for more than 10 hours. The Co and Ni cation in LDH can adsorb OH^- and undergo four electron transfer reaction. They are the active sites in which oxygen is generated. By introducing amorphous structure, this active sites can be fully exposed, so as to improve the performance of OER. This study provides an electrooxidation method to solve the drawbacks of LDH self-stacking effect, and opens up a new way to improve the catalytic performance of LDH catalyst.

Conflicts of interest

The authors declare there are no conflicts of interest regarding the publication of this paper.

Acknowledgements

The authors gratefully acknowledge financial support from by the Natural Science Foundation of Shandong Province of China (Grant No. ZR2020ME049).

References

1 M. A. Kirsanova, V. D. Okatenko, D. A. Aksyonov, R. P. Forslund, J. T. Mefford, K. J. Stevenson and A. M. Abakumov, *J. Mater. Chem. A*, 2019, 7, 330–341.

2 P. Lyu and P. Nachtigall, *Catal. Today*, 2020, **345**, 220–226.
3 J. Masud, S. Umapathi, N. Ashokaan and M. Nath, *J. Mater. Chem. A*, 2016, **4**, 9750–9754.
4 V. Pfeifer, T. E. Jones, S. Wrabetz, C. Massue, J. J. V. Velez, R. Arrigo, M. Scherzer, S. Piccinin, M. Havecker, A. Knop-Gericke and R. Schlogl, *Chem. Sci.*, 2016, **7**, 6791–6795.
5 A. T. Swesi, J. Masud and M. Nath, *Energy Environ. Sci.*, 2016, **9**, 1771–1782.
6 M. R. Gao, Y. F. Xu, J. Jiang and S. H. Yu, *Chem. Soc. Rev.*, 2013, **42**, 2986–3017.
7 M. Lewis, S. P. Neill, P. E. Robins and M. R. Hashemi, *Energy*, 2015, **83**, 403–415.
8 S. J. Wang, Z. Li, Y. Y. Zhang, X. R. Liu, J. Han, X. H. Li, Z. K. Liu, S. Liu and W. C. H. Choy, *Adv. Funct. Mater.*, 2019, **29**, 1900417.
9 L. Y. Zeng, K. A. Sun, X. B. Wang, Y. Q. Liu, Y. Pan, Z. Liu, D. W. Cao, Y. Song, S. H. Liu and C. G. Liu, *Nano Energy*, 2018, **51**, 26–36.
10 J. Kibsgaard and I. Chorkendorff, *Nat. Energy*, 2019, **4**, 430–433.
11 X. M. Li, X. G. Hao, A. Abudula and G. Q. Guan, *J. Mater. Chem. A*, 2016, **4**, 11973–12000.
12 S. M. Galani, A. Mondal, D. N. Srivastava and A. B. Panda, *Int. J. Hydrogen Energy*, 2020, **45**, 18635–18644.
13 B. T. Jebaslinhepzybai, T. Partheeban, D. S. Gavali, R. Thapa and M. Sasidharan, *Int. J. Hydrogen Energy*, 2021, **46**, 21924–21938.
14 S. P. Keerthana, B. J. Rani, G. Ravi, R. Yuvakkumar, S. I. Hong, D. Velauthapillai, B. Saravanakumar, M. Thambidurai and C. Dang, *Int. J. Hydrogen Energy*, 2020, **45**, 18859–18866.
15 S. Saha and A. K. Ganguli, *ChemistrySelect*, 2017, **2**, 1630–1636.
16 S. A. Chala, M. C. Tsai, W. N. Su, K. B. Ibrahim, B. Thirumalraj, T. S. Chan, J. F. Lee, H. J. Dai and B. J. Hwang, *ACS Nano*, 2020, **14**, 1770–1782.
17 C. L. Luan, G. L. Liu, Y. J. Liu, L. Yu, Y. Wang, Y. Xiao, H. Y. Qiao, X. P. Dai and X. Zhang, *ACS Nano*, 2018, **12**, 3875–3885.
18 A. Devadas, S. Baranton, T. W. Napporn and C. Coutanceau, *J. Power Sources*, 2011, **196**, 4044–4053.
19 F. L. Lyu, Q. F. Wang, S. M. Choi and Y. D. Yin, *Small*, 2019, **15**, 1804201.
20 S. Anantharaj, S. Kundu and S. Noda, *Nano Energy*, 2021, **80**, 105514.
21 R. Miao, B. Dutta, S. Sahoo, J. K. He, W. Zhong, S. A. Cetegen, T. Jiang, S. P. Alpay and S. L. Suib, *J. Am. Chem. Soc.*, 2017, **139**, 13604–13607.
22 R. L. Fan, Q. Q. Mu, Z. H. We, Y. Peng and M. R. Shen, *J. Mater. Chem. A*, 2020, **8**, 9871–9881.
23 B. J. Waghmode, A. P. Gaikwad, C. V. Rode, S. D. Sathaye, K. R. Patil and D. D. Malkhede, *ACS Sustainable Chem. Eng.*, 2018, **6**, 9649–9660.
24 X. Zhang, J. J. Fan, X. Y. Lu, Z. J. Han, C. Cazorla, L. Hu, T. Wu and D. W. Chu, *Chem. Eng. J.*, 2021, **415**, 129048.
25 L. Tian, K. Wang, H. X. Wo, Z. Li, M. Song, J. Li, T. X. Li and X. H. Du, *J. Taiwan Inst. Chem. Eng.*, 2019, **96**, 273–280.
26 Y. H. Liu, Y. Y. Chen, R. Y. Ge, W. X. Li, Y. Zhang, L. Y. Feng and R. C. Che, *Sustainable Mater. Technol.*, 2020, **25**, e00170.
27 Y. S. Tian, S. Y. Li, R. Q. Huang, Z. F. Wei, X. Ji, P. Liu, Y. J. Li and Q. S. Jing, *J. Alloys Compd.*, 2022, **899**, 163259.
28 X. H. Xu, L. Su, Y. J. Zhang, L. J. Dong and X. Y. Miao, *New J. Chem.*, 2021, **45**, 15429–15436.
29 L. Y. Hu, M. Y. Li, X. Q. Wei, H. J. Wang, Y. Wu, J. Wen, W. L. Gu and C. Z. Zhu, *Chem. Eng. J.*, 2020, **398**, 125605.
30 S. Y. Tee, C. J. J. Lee, S. S. Dinachali, S. C. Lai, E. L. Williams, H. K. Luo, D. Z. Chi, T. S. A. Hor and M. Y. Han, *Nanotechnology*, 2015, **26**, 415401.
31 T. Li, G. H. Li, L. H. Li, L. Liu, Y. Xu, H. Y. Ding and T. Zhang, *ACS Appl. Mater. Interfaces*, 2016, **8**, 2562–2572.
32 J. Wu, W. W. Liu, Y. X. Wu, T. C. Wei, D. S. Geng, J. Mei, H. Liu, W. M. Lau and L. M. Liu, *Electrochim. Acta*, 2016, **203**, 21–29.
33 H. F. Liang, F. Meng, M. Caban-Acevedo, L. S. Li, A. Forticaux, L. C. Xiu, Z. C. Wang and S. Jin, *Nano Lett.*, 2015, **15**, 1421–1427.
34 Q. Wang and D. O'Hare, *Chem. Rev.*, 2012, **112**, 4124–4155.
35 G. L. Fan, F. Li, D. G. Evans and X. Duan, *Chem. Soc. Rev.*, 2014, **43**, 7040–7066.
36 Z. L. Zhao, H. X. Wu, H. L. He, X. L. Xu and Y. D. Jin, *Adv. Funct. Mater.*, 2014, **24**, 4698–4705.
37 J. Jiang, A. L. Zhang, L. L. Li and L. H. Ai, *J. Power Sources*, 2015, **278**, 445–451.
38 S. F. Sun, C. D. Lv, W. Z. Hong, X. Zhou, F. G. Wu and G. Chen, *ACS Appl. Energy Mater.*, 2019, **2**, 312–319.
39 Y. Surendranath, M. W. Kanan and D. G. Nocera, *J. Am. Chem. Soc.*, 2010, **132**, 16501–16509.
40 Y. L. Shi, J. Q. Li, B. Y. Zhang, S. Y. Lv, T. Wang and X. Liu, *Appl. Surf. Sci.*, 2021, **565**, 150506.
41 Y. Y. Yang, Q. Zhou, L. Jiao, Q. Yin, Z. M. Li, Z. Y. Zhang and Z. A. Hu, *Ionics*, 2022, **28**, 341–351.
42 F. Dionigi, Z. H. Zeng, I. Sinev, T. Merzdorf, S. Deshpande, M. B. Lopez, S. Kunze, I. Zegkinoglou, H. Sarodnik, D. X. Fan, A. Bergmann, J. Drnec, J. F. de Araujo, M. Gliech, D. Teschner, J. Zhu, W. X. Li, J. Greeley, B. Roldan Cuenya and P. Strasser, *Nat. Commun.*, 2020, **11**, 2522.
43 M. Shakeel, M. Arif, G. Yasin, B. S. Li and H. D. Khan, *Appl. Catal., B*, 2019, **242**, 485–498.
44 E. Jung, J. K. Kim, H. Choi, M. H. Lee and T. Yu, *Dalton Trans.*, 2018, **47**, 17342–17348.
45 F. Song and X. L. Hu, *J. Am. Chem. Soc.*, 2014, **136**, 16481–16484.
46 H. Y. Meng, W. Xi, Z. Y. Ren, S. C. Du, J. Wu, L. Zhao, B. W. Liu and H. G. Fu, *Appl. Catal., B*, 2021, **284**, 119707.
47 F. K. Yang, K. Sliozberg, I. Sinev, H. Antoni, A. Bahr, K. Ollegott, W. Xia, J. Masa, W. Grunert, B. Roldan Cuenya, W. Schuhmann and M. Muhler, *ChemSusChem*, 2017, **10**, 156–165.
48 Q. B. Dong, C. Shuai, Z. L. Mo, N. J. Liu, G. G. Liu, J. Wang, H. B. Pei, Q. Q. Jia, W. T. Liu and X. D. Guo, *J. Solid State Chem.*, 2021, **296**, 121967.
49 W. M. Li, S. H. Chen, M. X. Zhong, C. Wang and X. F. Lu, *Chem. Eng. J.*, 2021, **415**, 128879.